ISSN 1560-3547, Regular and Chaotic Dynamics, 2017, Vol. 22, No. 5, pp. 551–565. © Pleiades Publishing, Ltd., 2017.

A Family of Models with Blue Sky Catastrophes of Different Classes

Pavel V. Kuptsov[1*], Sergey P. Kuznetsov[2], and Nataliya V. Stankevich[1,3***]**

[1] *Yuri Gagrin State Technical University of Saratov*
ul. Politehnicheskaya 77, Saratov, 410054 Russia

[2] *Kotel'nikov's Institute of Radio-Engineering and Electronics of RAS, Saratov Branch*
ul. Zelenaya 38, Saratov, 410019 Russia

[3] *University of Jyväskylä*
Mattilanniemi 2, FIN-40014, Finland

Received August 17, 2017; accepted September 08, 2017

Abstract—A generalized model with bifurcations associated with blue sky catastrophes is introduced. Depending on an integer index m, different kinds of attractors arise, including those associated with quasi-periodic oscillations and with hyperbolic chaos. Verification of the hyperbolicity is provided based on statistical analysis of intersection angles of stable and unstable manifolds.

MSC2010 numbers: 34C28, 34C23, 37D20, 37E99, 37G15, 37G35

DOI: 10.1134/S1560354717050069

Keywords: dynamical system, blue sky catastrophe, quasi-periodic oscillations, hyperbolic chaos, Smale – Williams solenoid

INTRODUCTION

Originally, the bifurcation called the blue sky catastrophe was described in [1]. In the simplest case it can be explained as follows. The phase trajectory departs from a vicinity of a semistable limit cycle (saddle-node periodic orbit) existing at the threshold of the bifurcation, goes around a large-size loop, and turns back to the limit cycle from the other side. As a control parameter is varied in one direction, the semistable cycle transforms into a pair of cycles, a stable and an unstable one. As the control parameter is varied in the opposite direction, two cycles meet each other, forming the semistable cycle, and then disappear, while the large-size limit cycle emerges in the domain of the above-mentioned loop containing helical coils in the phase space region of the former limit cycle pair (Fig. 1a). Conditions and mechanisms of birth of limit cycles through the blue sky catastrophe are described in detail in [2–8].

According to the analysis developed in [2], it is natural to consider actually a family of such bifurcations distinguished by an integer index m. Indeed, in general, if a phase trajectory with some angular coordinate φ departs from the saddle-node cycle, then after a travel along the large-size loop and subsequent return it will be characterized by this angular coordinate expressed by a relation containing an additive term of form $m\varphi$ (Fig. 1b). For three-dimensional phase space (the minimal dimension where the blue-sky catastrophe may take place) the integer m may be either 0 or 1. However, at higher dimensions, any integer can occur. In particular, $m = 2$ will correspond to the birth of a hyperbolic strange attractor represented by a classical Smale–Williams solenoid in a Poincaré section, and $m > 2$ to solenoids of larger rates of increase in the number of loops at successive stages of their geometric construction [3] (Fig. 2).

*E-mail: p.kuptsov@rambler.ru
**E-mail: spkuz@yandex.ru
***E-mail: stankevichnv@mail.ru

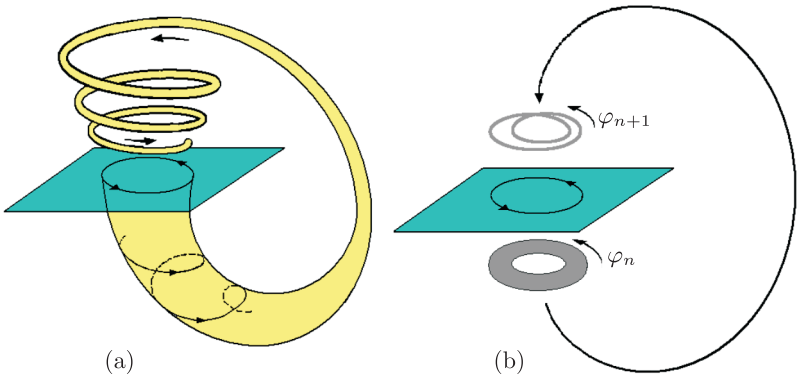

Fig. 1. Phase space structure in the case of the blue sky catastrophe in the simplest case of three dimensions (a) and schematic representation of the situation where the Smale–Williams attractor can appear in a phase space of dimension 4 and higher (b).

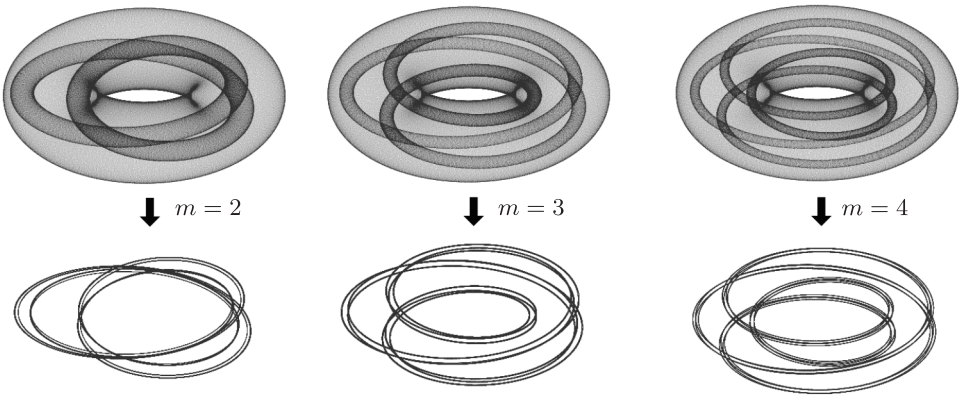

Fig. 2. Formal geometric construction of the Smale-Williams solenoids associated with the indices $m = 2$, 3, and 4: initial toroidal domain in the state space, results of its transformation in the first iteration of the mapping, and the solenoid obtained after a large number of repetitive applications of the procedure.

In a series of works, different applications were discussed in relation to the blue sky catastrophes. Remarkably, a lot was done in connection with biological models and neurons. For instance, some results demonstrating a transition between tonic-spiking and bursting in a model of leech neuron are presented in reference [9]. Also, in [10–12] it was mentioned that this kind of bifurcation can be considered as the main mechanism for the onset of the burst-spike dynamics, and it was observed in other neuron-like models. Such approaches were applied for relaxation systems with fast and slow variables, and for modeling the cardiac rhythms [13, 14]. In a recent paper [15] the authors suggest that the interaction of technology and economic policy regulations in the energy sector may be described by slow-fast systems, where the blue sky catastrophes are possible. In [16] the bifurcation associated with the blue sky catastrophe was considered as one of scenarios for the birth of chimera states in ensembles of phase oscillators, which are used for description networks of neurons and for other biological models of interaction.

In [17] the bifurcation of the blue sky catastrophe has been found in a binary mixture contained in a laterally heated cavity at small Prandtl numbers. In [18–20] the blue sky catastrophes are discussed in relation to astrophysics, in the context of the restricted four-body problem. In [21] results are presented concerning maps describing the Josephson junction, where such kind of bifurcation was observed. In [22] a blue sky catastrophe of limit cycles of van der Pol system with noise (fuzzy disturbance) was studied.

Also, theoretical investigations of the blue sky catastrophes continue to develop [23–26]. Most of these studies relate to the simplest case of the limit cycle birth in the bifurcation (index $m = 0$ according to the classification of reference [2]).

However, no concrete examples relating to the emergence of hyperbolic chaos have been considered, although recently a number of models and experimental electronic circuits manifesting this phenomenon have been proposed [27–29, 32, 33].

In the context of the present study, the most important is the four-dimensional system, in which an attractor of Smale – Williams type appears as a result of the blue sky catastrophe with the Turaev – Shilnikov index $m = 2$, which was suggested and studied numerically in reference [33]. By modifying this system, it is possible to construct models with other integer indices m representing various types of the blue-sky catastrophes; particularly, in reference [34] we considered the case $m = 1$ associated with the birth of quasi-periodicity.

In the present work we suggest a generalized model representing a family of four-dimensional dynamical systems, in which the blue sky catastrophes of different classes outlined by Turaev and Shilnikov [2, 3] take place. In Section 2 we introduce a model manifesting the blue sky catastrophes containing an index m as an integer parameter, depending on what kinds of attractors can arise due to the bifurcations. In Section 3 we review possible dynamical regimes of the model and discuss the structure of the space of control parameters. In Section 4 we consider a generalized model in the case of emergence of quasi-periodic dynamics $m = 1$. In Section 5 results of numerical simulation of the generalized model with $m = 2, 3, 4$ are presented, and the occurrence of hyperbolic chaos is demonstrated. In Section 6 we present results of verification of hyperbolicity based on analysis of statistical distributions of the angles of intersection of stable and unstable manifolds of orbits on the attractors.

1. FAMILY OF SYSTEMS WITH THE BLUE SKY CATASTROPHES

In order to construct a generalized model, let us start with a two-dimensional predator–prey system with instant state specified by two nonnegative variables r_1, r_2:

$$\begin{aligned} \dot{r}_1 &= 2\left(1 - r_2 + \frac{1}{2}r_1 - \frac{1}{50}r_1^2\right) r_1, \\ \dot{r}_2 &= 2\left(r_1 - \mu + \frac{1}{2}r_2 - \frac{1}{50}r_2^2\right) r_2. \end{aligned} \tag{1.1}$$

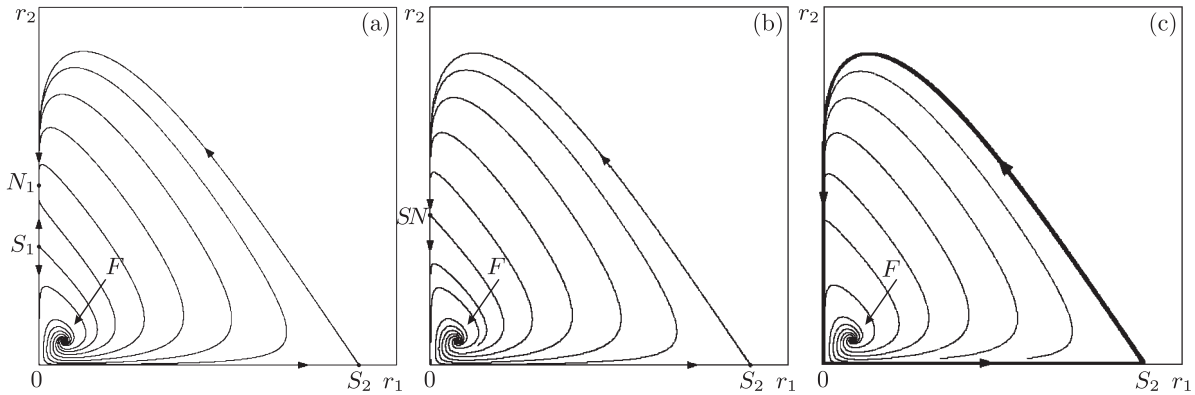

Fig. 3. Phase portraits of the system (1.1); diagrams from (a) to (c) correspond to increase in parameter μ.

These equations differ from those in reference [29] with additional nonlinear terms in the second ("predator") equation, and contain a control parameter μ. If the value of μ is slightly less than $\mu_0 = 3\frac{1}{8}$, the picture of orbits on the phase plane (r_1, r_2) looks like that shown in Fig. 3a. There are four fixed points here, an unstable focus F, saddles S_1 and S_2, and a node N_1. With increasing μ, the fixed points S_1 and N_1 move to meet each other at $\mu = \mu_0$, and then disappear (see panels (b) and (c), respectively). Instead of the former pair of fixed points, a domain of relatively slow motion appears there, while the attractor is a limit cycle, which passes close to the origin and to the saddle S_2.

Following [29], let us consider the quantities r_1 and r_2 as squared absolute values of complex amplitudes for two oscillators of some frequency ω_0, namely, $r_{1,2} = |a_{1,2}|^2$. One can write down a set of differential equations for the complex variables a_1 and a_2 and add terms of a certain form, which introduce an additional coupling between the oscillators in the following way:

$$\begin{aligned} \dot{a}_1 &= -i\omega_0 a_1 + \left(1 - |a_2|^2 + \frac{1}{2}|a_1|^2 - \frac{1}{50}|a_1|^4\right) a_1 + \frac{1}{2}\varepsilon \operatorname{Im} a_2^m, \\ \dot{a}_2 &= -i\omega_0 a_2 + \left(|a_1|^2 - \mu + \frac{1}{2}|a_2|^2 - \frac{1}{50}|a_2|^4\right) a_2 + \varepsilon \operatorname{Re} a_1. \end{aligned} \tag{1.2}$$

Here ε is a coupling coefficient and m is an integer index. At $\varepsilon = 0$, the equations for $r_{1,2} = |a_{1,2}|^2 = x_{1,2}^2 + y_{1,2}^2$ derived from (1.2) coincide precisely with Eqs. (1.1). At ε small enough, and at values of μ notably less than μ_0, the sustained dynamics presented graphically on the plane (r_1, r_2) is located close to the node N_1. For nonzero ε, this is a limit cycle of such kind that the second oscillator has some notable amplitude, while for the first one the amplitude is very small. Besides, there is an unstable limit cycle close to S_1. With gradual increase of the parameter, both cycles come closer, meet together and coincide at some $\mu = \mu_c(\varepsilon) \approx \mu_0$, forming a semistable limit cycle. At $\mu > \mu_c(\varepsilon)$ it disappears. Now the motion of a representative point on the plane (r_1, r_2) follows approximately a closed large-scale path, as in Fig. 3c, visiting again and again a neighborhood of the origin. Qualitatively, for each such passage, the following stages may be specified: excitation of the first oscillator (i), excitation of the second oscillator (ii), damping of the first oscillator (iii), and slower damping of the second oscillator (iv). Activation of the second oscillator occurs in the presence of driving from the partner, due to the coupling term proportional to ε in the second equation, so it inherits the phase from the first oscillator. During the damping stage of the second oscillator, its residual oscillations initiate the activation of the first one. The corresponding term proportional to ε in the first equation contains complex amplitude in the power of m, so this transfer of excitation is accompanied with multiplication of the argument of the complex variable that is the phase of the oscillations. Then the process repeats again and again. So the transformation of the phase at each next cycle of the excitation exchange corresponds to the circle map,

$$\varphi_{n+1} = m\varphi_n + \text{const}, \tag{1.3}$$

which is expanding for $m \geqslant 2$. At $m = 2$ it is commonly referred to as the Bernoulli map. Then let us analyze dynamical regimes in the model (1.2) for different m.

2. DYNAMICAL BEHAVIOR OF THE GENERALIZED MODEL

One of the well-known techniques for studies of dynamical systems is the method of charts of dynamical regimes [30, 31], which reveals the disposition of dynamical regimes depending on control parameters visualizing the parameter plane topography. Let us consider the system (1.2) using this method. As the control parameters we choose the basic frequency of the self-oscillations ω_0 and the parameter μ responsible for the transition through the blue sky bifurcation. We note that the index m is not regarded as a control parameter in the classical sense, since the differential equations are modified if we change m. Undertaking the computations, for each value of m we deal with a concrete four-dimensional set of differential equations (In the Appendix full representations of the equations are collected with different values of m).

Figure 4 shows the charts of dynamical regimes for $m = 1$ (a), $m = 2$ (b), $m = 3$ (c), and $m = 4$ (d). In the course of plotting the charts, for periodic regimes we evaluate the number of discrete points in the Poincaré section by a surface $\operatorname{Re}(a_1) = 0$ after excluding transients. (The legend for correspondence of the periods and colors is given in the bottom part of Fig. 4). In the case of the number of discrete points larger than 120, we regard the regime as nonperiodic (which may be either chaotic or quasi-periodic), and the respective point of the parameter plane is colored by a certain gray color tone.

For all values of m from 1 to 4, on the parameter planes of Fig. 4 one can observe two kinds of characteristic bifurcation lines, at which complex dynamics emerge. The first line $\mu_c^{BS} \approx 3\frac{1}{8}$ is that corresponding to the bifurcation of the blue sky catastrophe. The second line $\mu_c^{NS} \approx 16.5$ is that

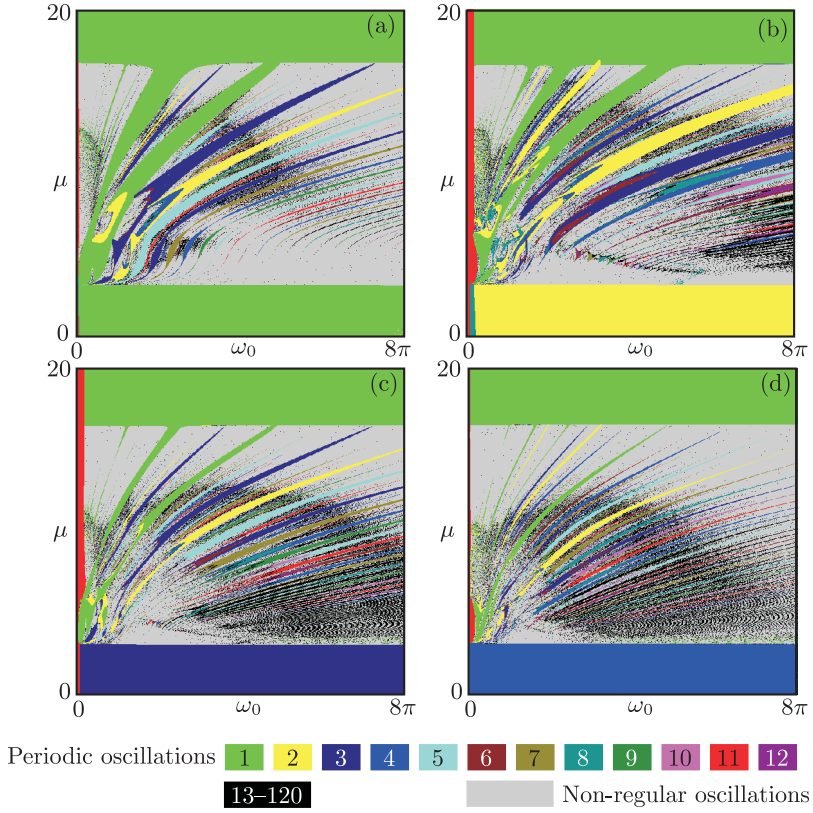

Fig. 4. Charts of dynamical regimes for the generalized model (1.2) at (a) $m = 1$, $\varepsilon = 1$; (b) $m = 2$, $\varepsilon = 0.5$; (c) $m = 3$, $\varepsilon = 0.1$; (d) $m = 4$, $\varepsilon = 0.02$.

of the Neimark – Sacker bifurcation. Arrangements of the parameter plane for all discussed values of m look similar: for $\mu_c^{NS} < \mu < \mu_c^{BS}$ periodic self-oscillations take place; inside the band between μ_c^{BS} and $\mu < \mu_c^{NS}$ there is a complex structure including resonance tongues and nonperiodic self-oscillations.

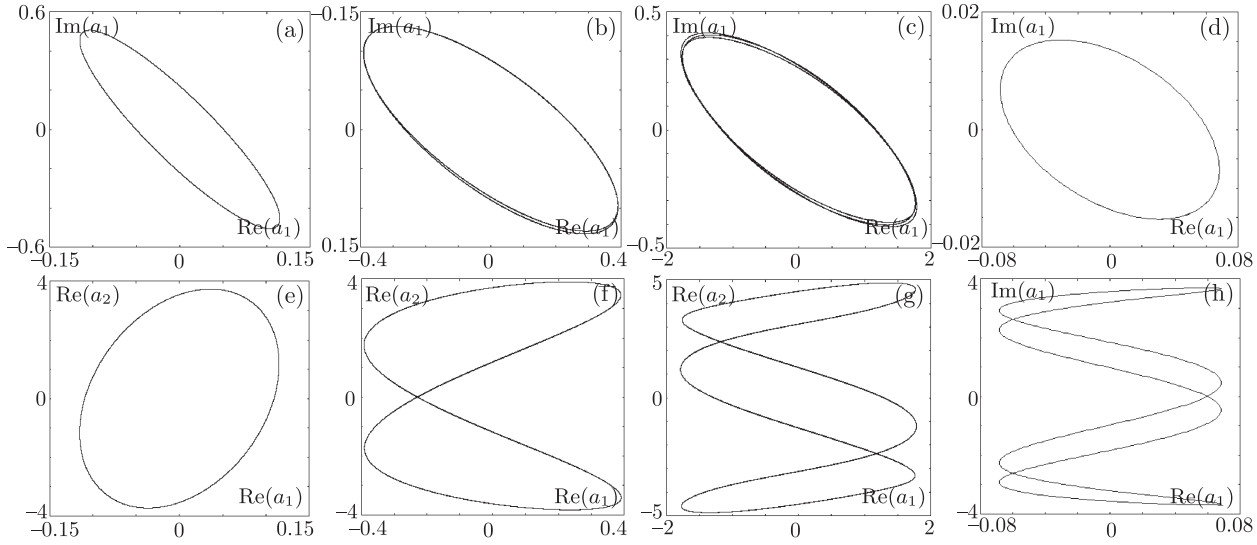

Fig. 5. Two-dimensional projections of phase portraits and Lissajous figures for the model (1.2) before the bifurcation of the blue sky at $\mu = 3.1$, $\omega_0 = 2\pi$, (a) $m = 1$, $\varepsilon = 1$; (b) $m = 2$, $\varepsilon = 0.5$; (c) $m = 3$, $\varepsilon = 0.1$; (d) $m = 4$, $\varepsilon = 0.02$.

Periods of the regimes occurring before the blue sky catastrophe ($\mu < \mu_c^{BS}$) differ depending on the index m. In Fig. 5 we show the corresponding two-dimensional projections of phase portraits on the plane of real and complex parts of the amplitude of the first oscillator $\big(\Re(a_1), \Im(a_1)\big)$ and two-dimensional projections of Lissajous figures on the planes of real parts of amplitudes of the first and the second oscillators $\big(\Re(a_1), \Re(a_2)\big)$. On the projections of phase portraits the observed numbers of rotation for the orbits correspond to the index m. On the projections of the Lissajous figures with increase of the index m one can see the appearance of self-intersections of the trajectory; the number of self-intersections is equal to $m - 1$.

Inside the area between the bifurcation lines μ_c^{BS} and μ_c^{NS} sets of synchronization tongues occur on the parameter plane, and among them one can distinguish main tongues of period 1. The upper bases of the tongues are placed along the Neimark – Sacker bifurcation line; the last tongue of period-1 is located on the parameter plane at frequency $\omega_0 = 4.8\pi$, other tongues at $\omega_{02} = \omega_0/2$, $\omega_{03} = \omega_0/3$, $\omega_{04} = \omega_0/4$, $\omega_{05} = \omega_0/5$, $\omega_{06} = \omega_0/6$; the frequencies of the successive tongues decrease geometrically. Between the period-1 tongues, narrower tongues of higher order are observed. The bottom base of the main diagonal line of period-1 ($\omega_0 = 4.8\pi$) leans on the line of bifurcation associated with the blue sky catastrophe; to the right of this only resonances of higher orders are observed, but to the left of this the same repeating structures of tongues are observed, which lean on the main diagonal tongue of period-1 instead of the line of blue sky catastrophe.

Apart from that, we discuss quasi-periodic and chaotic oscillations (domains of gray color on the parameter planes). As mentioned above, the horizontal line $\mu_c^{NS} \approx 16.5$ corresponds to the Neimark – Sacker bifurcation; as a result of this bifurcation a two-dimensional torus emerges for any m as we go downward in the parameter plane. Tongues of synchronization with different winding numbers lean on the line of the Neimark – Sacker bifurcation. With decreasing μ the synchronization tongues overlap, and chaotic dynamics develops. Inside several tongues one can observe transition to chaos via period-doubling bifurcation cascades.

The structure of the parameter plane near the line of bifurcation of the blue sky catastrophe differs essentially for different m. The synchronization tongues at the bottom bifurcation line tighten at one point. Note that the formation of complex dynamics in the course of the blue sky bifurcation has specific features for different values of index m. For example, for $m = 1$ one can see that the synchronization tongues of high order approach very close the bifurcation line and tend to one point along this line (Fig. 4a). It was checked in [34] that for this case, as a result of the blue sky catastrophe, a two-frequency torus is born; see also Section 4. For $m = 2, 3, 4$ one can see homogeneous domains of chaotic dynamics (gray color) on the parameter planes above the bifurcation line of blue sky catastrophe in several intervals of ω_0, which correspond to robust hyperbolic chaos (Figs. 4b–4d). In Section 5 we consider in detail the features of formation of hyperbolic chaos. In Section 6 we present results of computer verification of the hyperbolicity.

3. QUASI-PERIODIC DYNAMICS

Quasi-periodic oscillations are typical of systems of coupled oscillators. As one can see from Fig. 4, quasi-periodic dynamics take place in the generalized model (1.2), arising as a result of the Neimark – Sacker bifurcation for $\mu_c^{NS} \approx 16.5$. The topography of the parameter plane has a specific characteristic structure manifesting sets of tongues of synchronization on multiple frequencies embedded in the area of quasi-periodicity.

In Fig. 6 two-dimensional projections (gray color) and Poincaré sections (black color) of typical phase portraits for the generalized model (1.2) are presented for different values of index m. Projections of the attractors are projections of tori. In the Poincaré section an invariant curve is visualized[1)].

Quasi-periodic oscillations in the model (1.2) with index $m = 1$ occur as a result of the blue sky catastrophe. Figure 7 shows a two-dimensional projection of phase portrait (a), and its Poincaré section formed by the intersection with the surface $\mathrm{Re}(a_1) = 0$ (b). In the Poincaré section we observe a smooth invariant curve. The diagram in panel (c) demonstrates the evolution of phases at successive crossings of the surface $|a_1| = |a_2|$ corresponding to the Poincaré section in the correct

[1)] For this case we realized the Poincaré section by the surface $\mathrm{Re}(a_1) = 0$.

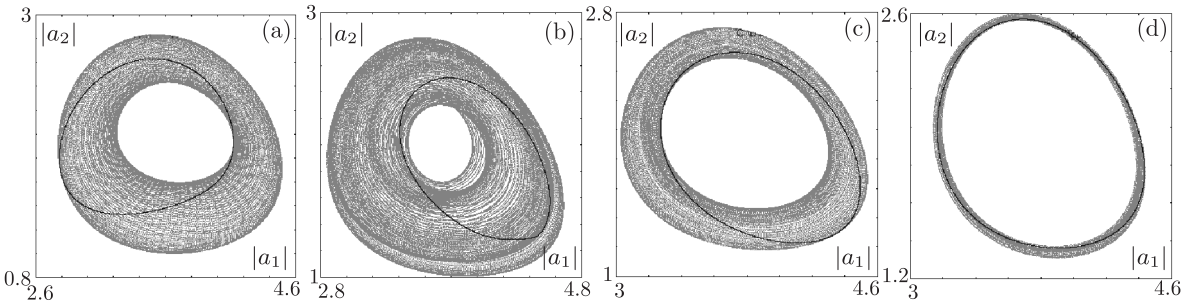

Fig. 6. Two-dimensional projections (gray) and Poincaré sections formed by the intersection with the plane $\mathrm{Re}(a_1) = 0$ of two-frequency quasi-periodic oscillations born as a result of the Neimark – Sacker bifurcation, (a) $m = 1$, $\varepsilon = 1$, $\omega_0 = 3\pi$, $\mu = 16$; (b) $m = 2$, $\varepsilon = 0.5$, $\omega_0 = 2\pi$, $\mu = 16$; (c) $m = 3$, $\varepsilon = 0.1$, $\omega_0 = 2\pi$, $\mu = 16$; (d) $m = 4$, $\varepsilon = 0.02$, $\omega_0 = 2\pi$, $\mu = 16$.

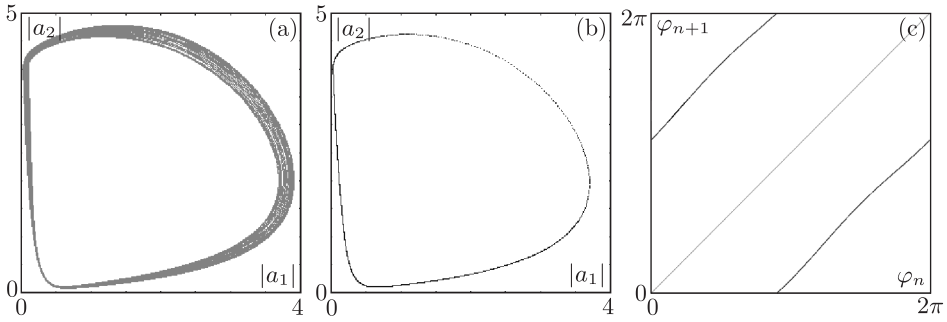

Fig. 7. Two-dimensional phase portrait (a) and its Poincaré section (b) for a quasi-periodic regime; (c) map of phases for the first oscillator in the Poincaré section formed by the intersection with the plane $|a_1| = |a_2|$, for $m = 1$, $\varepsilon = 1$, $\omega_0 = 3\pi$, $\mu = 3.15$.

direction of increase of $|a_2|$. The phase φ_n relates to the first oscillator at $t = t_n$, which is the nth crossing. In computations, it is determined as $\varphi_n = \arg\big(a_1(t_n)\big)$. The plot for the map of phases contains two almost parallel lines, without intersection with the bisector, and it looks like the map (1.3) for $m = 1$.

4. HYPERBOLIC CHAOS AND OTHER PHENOMENA

According to the theory of Shilnikov and Turaev, for $m \geqslant 2$ hyperbolic chaos is expected in the system. Now we consider some features of formation of the hyperbolic chaotic attractors.

As mentioned above, in Figs. 4b–4d nearly above the boundary line of the blue sky catastrophe bifurcation line one can observe chaotic dynamics that correspond at $m \geqslant 2$ to regimes of hyperbolic chaos. Consider some illustrations of this kind of dynamics.

Figure 8 shows two-dimensional projections of phase portraits in the regime of hyperbolic chaos for m from 2 to 4 (top row) together with the respective iterative diagrams for phases at successive passages of the Poincaré section formed by the intersection with the surface $|a_1| = |a_2|$. Observe that for $m = 2$ topologically the discrete-step evolution of the phases corresponds to the Bernoulli map: one full revolution for the preimage φ_n gives rise to two revolutions for the image φ_{n+1}. For $m = 3$ and $m = 4$ the transformation of the phases corresponds to the triple and quadruple expanding circle map (1.3): one full revolution for the preimage φ_n gives rise to three and four revolutions for the image φ_{n+1}, respectively. It supports the qualitative arguments that the case $m \geqslant 2$ occurs here, associated with the presence of the Smale – Williams solenoid in the Poincaré map according to the Shilnikov – Turaev theory.

Figure 9 shows, for the same values of parameters, the waveforms produced by two oscillators constituting the system. Here we observe the process of exchange of excitation between the subsystems according to its description in Section 2. The waveforms of the second subsystem are smooth enough, and those of the first one have small-scale oscillations near zero, while the second

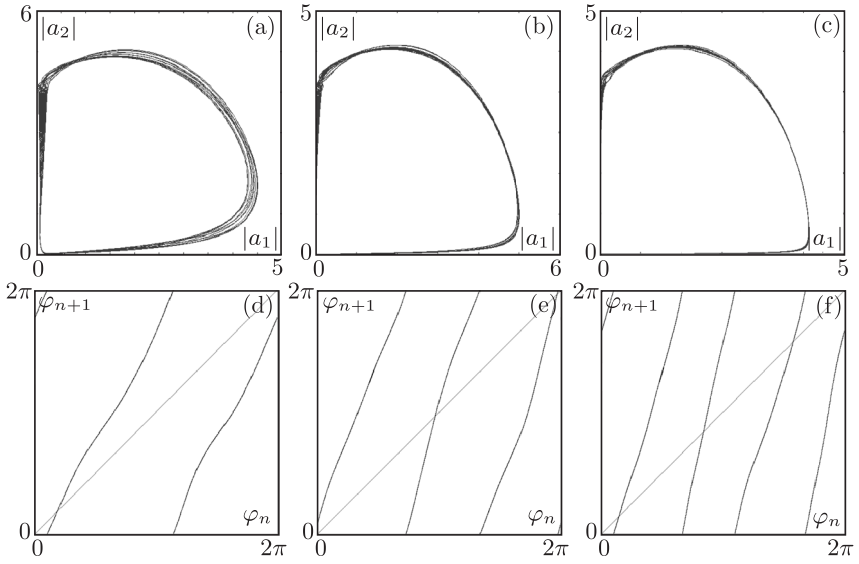

Fig. 8. Two-dimensional projections of phase portraits and the map of phases of the generalized model (1.2) in the regime of hyperbolic chaos for different values of index m: (a) $m = 2$, $\varepsilon = 0.5$, $\omega_0 = 2\pi$, $\mu = 3.15$; (b) $m = 3$, $\varepsilon = 0.1$, $\omega_0 = 2\pi$, $\mu = 3.15$; (c) $m = 4$, $\varepsilon = 0.02$, $\omega_0 = 2\pi$, $\mu = 3.15$.

subsystem has a large amplitude. They correspond to oscillations on the helical coils, which occur in the vicinity of the small-scale limit cycles before the blue sky catastrophe. These fluctuations are well seen in two-dimensional projections of phase portraits in Fig. 8.

Let us consider in detail each case of different values of index m. Firstly, we turn to a one-parameter analysis. In Fig. 10a bifurcation diagrams for $m = 2$ and $\omega_0 = 3\pi$ are shown. In Figs. 10b and 10c magnified fragments are presented for vicinities of critical values of control parameters μ_c^{BS} and μ_c^{NS}. As in the case $m = 1$, near the Neimark – Sacker bifurcation a soft birth of a torus takes place. In the vicinity of the blue sky bifurcation, a hard birth of a two-frequency torus occurs.

Figure 10d–10i shows two-dimensional projections of phase portraits in the Poincaré section formed by the intersection with the plane $\mathrm{Re}(a_1) = 0$. As one can see, at $\mu = 3.15$ in the Poincaré section the phase portrait is close to a smooth invariant curve, but it has a small loop extending from the invariant curve. With increasing μ this loop grows, but in the diagrams for phases corresponds topologically to the Bernoulli map (Figs. 10e and 10j, $\mu = 4.3$). When we observe the transition to nonhyperbolic chaos in the bifurcation diagram, in the Poincaré section this loop becomes larger, and the map of phases becomes more complex and ceases to correspond to the Bernoulli map (Figs. 10f and 10k, $\mu = 6.3$). As one goes up to the Neimark – Sacker bifurcation line, this loop in the Poincaré section disappears gradually. For the quasi-periodic regime ($\mu = 12$) the iterative diagram of phases tends to a straight line of unit slope.

Now let us turn to two-parametric analysis and consider in more detail the structure of the parameter plane in the domain where hyperbolic chaos takes place. Figure 11 shows magnified fragments of the chart of dynamical regimes of the model (1.2) for values of index m from 2 to 4. A wide homogeneous domain of gray color corresponds to hyperbolic chaos. Thus, with increasing parameter μ, at μ_c^{BS} hyperbolic chaos emerges. With further increase of μ tongues of synchronization appear on the charts, which gradually become wider and start to overlap. This process accompanies the destruction (collapse) of hyperbolic chaos.

In [35], one of possible scenarios of birth and collapse of strange hyperbolic attractors associated with Smale – Williams solenoids was suggested. The outlined mechanism of transition, as the control parameter is varied, consists in merging orbits belonging to the attractor with orbits belonging to the unstable invariant set, which are in one-to-one correspondence, in some parameter interval of finite width through saddle-node bifurcations. The same type of behavior is observed in the generalized model (1.2) for values of index m from 2 to 4.

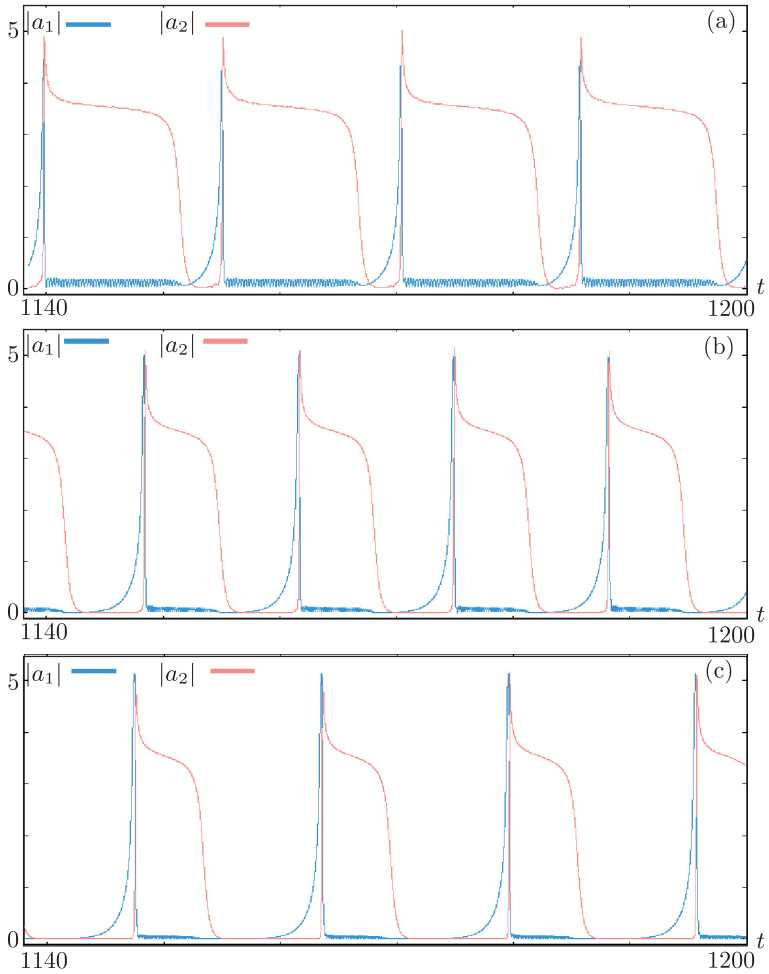

Fig. 9. Waveforms produced by the generalized model (1.2) in regimes of hyperbolic chaos for different values of index m: (a) $m = 2$, $\varepsilon = 0.5$, $\omega_0 = 2\pi$, $\mu = 3.15$; (b) $m = 3$, $\varepsilon = 0.1$, $\omega_0 = 2\pi$, $\mu = 3.15$; (c) $m = 4$, $\varepsilon = 0.02$, $\omega_0 = 2\pi$, $\mu = 3.15$.

5. LYAPUNOV EXPONENTS AND VERIFICATION OF HYPERBOLICITY

Consider Lyapunov exponents for the flow system (1.2) at different m, employing the standard algorithm [36, 37]. The computed values of the exponents λ_i, $i = 1, \ldots, 4$ are collected in Table 1. Note that for all three cases $m = 2, 3$ and 4 there is only one positive Lyapunov exponent. The second one is zero within a numerical error. Using the Lyapunov exponents, we can estimate the attractor dimension via the Kaplan – Yorke formula [38], see column D_{KY} in Table 1. Observe that the dimensions are remarkably close to each other for all three cases.

Table 1. Lyapunov exponents and Kaplan – Yorke dimension for the system (1.2) and the corresponding Poincaré map.

m	λ_1	λ_2	λ_3	λ_4	D_{KY}	Λ_1	T	$\lambda_1 T$
2	0.0439	−0.0001	−8.7588	−8.8606	2.0050	0.6793	15	0.6590
3	0.0810	−0.0001	−5.9709	−6.3186	2.0136	1.0729	14	1.1346
4	0.0817	−0.0003	−4.6255	−5.0960	2.0176	1.3635	17	1.3890

To perform the hyperbolicity test, a Poincaré map is required that represents the states of the flow system at successive excitation stages. We define this map in the same way as it was done previously, when the iteration diagrams for phases were plotted, with the section surface $|a_1| = |a_2|$.

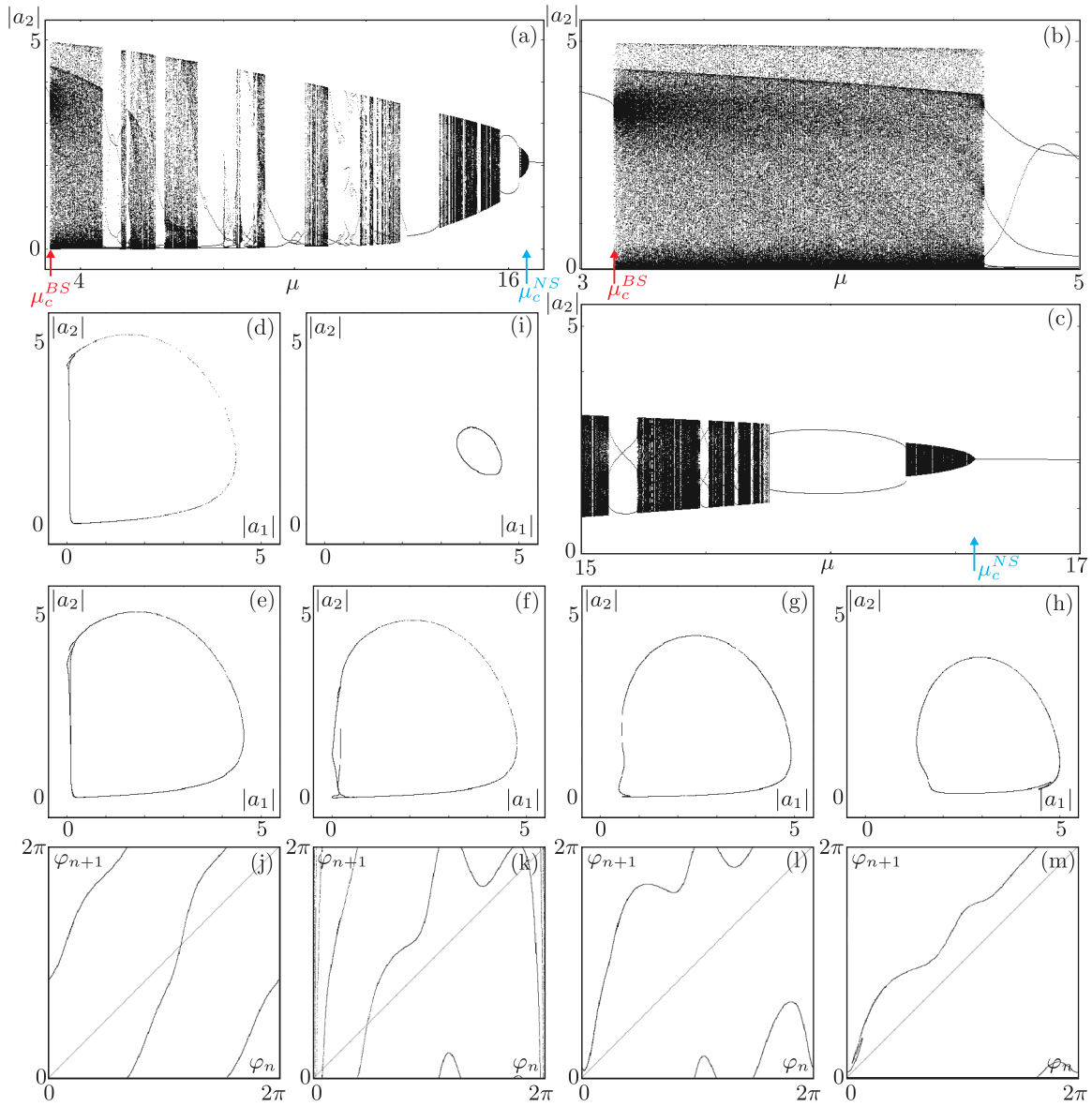

Fig. 10. Bifurcation diagrams and their magnified fragments in the vicinity of bifurcation lines of the generalized model (1.2) for $m = 2$, $\omega_0 = 3\pi$ (a)–(c); two-dimensional projections of phase portraits in the Poincaré section formed by the intersection with the plane $\mathrm{Re}(a_1) = 0$ for different values of parameter μ: (d) $\mu = 3.15$, (e) $\mu = 4.3$, (f) $\mu = 6.1$, (g) $\mu = 8.8$, (h) $\mu = 12.0$, (i) $\mu = 16.0$; and the corresponding map of phases (j) $\mu = 4.3$, (k) $\mu = 6.1$, (l) $\mu = 8.8$, (m) $\mu = 12.0$.

The comparison of the Lyapunov exponents for the map with exponents for the original flow system requires an average time T between the excitation stages, or, which is the same, between the Poincaré section crossings. We have computed it by analyzing the trajectories of the flow system; see the corresponding column in Table 1. Observe that the product $\lambda_1 T$ equals approximately the corresponding Λ_1.

The first Lyapunov exponent for the Poincaré map, see column Λ_1 of Table 1, equals approximately $\ln m$.

Let us now turn to the numerical test of hyperbolicity. The fast method of angles will be applied, see reference [39] for details. In reference [40] the theoretical background for this method is formulated.

All trajectories on a chaotic hyperbolic attractor are known to be of saddle type. This means that their manifolds, i.e., expanding, contracting and neutral, if any, always intersect transversally,

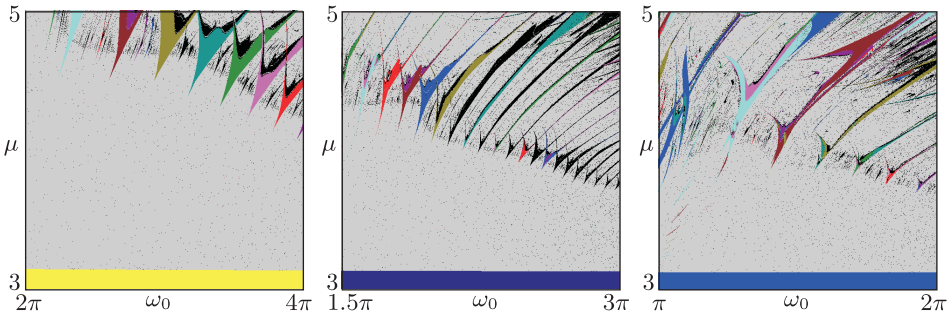

Fig. 11. Magnified fragments of the charts of dynamical regimes for the model (1.2) with $m = 2$ (a), 3 (b), and 4 (c), which contain the areas of hyperbolic chaos and their vicinities.

and no tangencies between them can occur. The method of angles consists in testing for this property: moving along a trajectory, we compute the angles between the subspaces tangent to the trajectory manifolds. The hyperbolicity is confirmed if the angles never vanish, while for nonhyperbolic attractors zero angles are encountered with a nonzero probability.

The fast method of angles [39] consists in passing forward and back in time along the same trajectory. The forward-time pass is identical with that performed for the Lyapunov exponents computation. The equations under consideration are integrated simultaneously with a required number, say K, of copies of the corresponding variation equations. Periodically, the orthonormalization of a matrix whose columns are solutions of the variational equations is performed. But unlike the routine for Lyapunov exponents, the matrices after the orthonormalizations are saved for further use.

For the backward-time pass, an adjoint variational equation has to be derived. For the system under consideration we merely have to transpose the Jacobian matrix and invert its sign. The adjoint variational equations are integrated in backward time. The number of equations is the same as on the forward pass, i. e., K. In quite the same way solutions of the adjoint equations provide columns of the matrix, which have to be periodically orthonormalized. This has to be done exactly at the same trajectory points as on the forward pass. The resulting orthogonal matrices together with the corresponding matrices saved on the forward pass are used for computation of the angles. A matrix of pairwise inner products of their columns is built; then for each of its top left submatrices the smallest singular value σ_i is computed, where $i = 1, \ldots, K$, and the angle is computed as $\theta_i = \frac{\pi}{2} - \arccos(\sigma_i)$ [39].

As discussed above, the flow systems with $m = 2, 3, 4$ exhibit chaotic regimes with one positive Lyapunov exponent, and due to the invariance under time shifts the second exponent is zero, see Table 1. This means that the respective trajectories have one-dimensional expanding and one-dimensional neutral manifolds. As we deal with the Poincaré map, we exclude the neutral manifold from consideration. Thus, testing the hyperbolicity, we need to compute the angle between expanding and contracting manifolds only. However, to actually exclude the neutral manifold in the course of computations, we should project the solutions of the variational and adjoint equations onto the Poincaré section surface, which complicates the routines. Instead we check if the original flow system on the section surface fulfills the conditions imposed on Anosov flows [41, 42]. This automatically implies hyperbolicity for the corresponding Poincaré map.

Thus, we need to compute two angles for the flow system: θ_1 between the expanding subspace and a direct sum of the neutral and contracting subspaces, and θ_2 between a direct sum of the expanding and neutral subspace and the contracting subspace. This means that $K = 2$, i. e., we need to solve two copies of the variational as well as the adjoint equations. The hyperbolicity will be confirmed if both of these angles never vanish.

Figures 12a–12c show the distributions of angles θ_1 and θ_2 computed for the system (1.2) $m = 2, 3$ and 4, respectively. In all three cases the distributions are well separated from the origin, which confirms the hyperbolicity of the corresponding attractors.

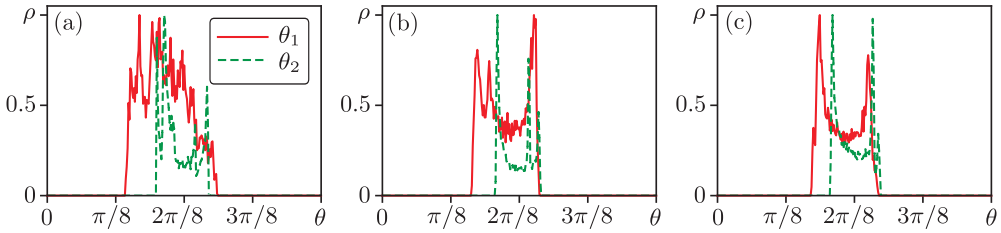

Fig. 12. Distributions of angles between subspaces tangent to trajectory manifolds of the system (1.2). Panels (a), (b) and (c) correspond to $m = 2$, 3 and 4, respectively. The parameters correspond to those given in the caption of Fig. 9. Angles are computed on the Poincaré section surface. The clear separation of the distributions confirms the hyperbolicity of the corresponding Poincaré map in all three cases.

6. CONCLUSIONS

We have introduced a family of systems governed by ordinary fourth-order differential equations in which, depending on an integer index m, different variants of the blue sky catastrophe occur. The latter is a bifurcation event consisting in the appearance of a large-scale attractor after merging and disappearance of a pair of small-scale stable and unstable limit cycles, when a control parameter is varied. In accordance with the Shilnikov – Turaev theory, the type of the resulting attractor is determined by the index m; its role is that it determines the m-fold expansion for an angular variable acquired by the trajectory at the entrance to the region of spiral movements in the phase space, where the former missing pair of limit cycles existed, in comparison with its initial value at the exit from that region. The cases $m = 1, 2, 3, 4$ are discussed in some detail. For $m = 1$, the result of bifurcation is the emergence of an attractive torus, and for $m \geqslant 2$ the result is the appearance of hyperbolic chaos associated with the attractor corresponding to a Smale – Williams solenoid in the Poincaré map. The topological type of the solenoid is determined by the index m, which characterizes the rate of increase in the number of loops of the solenoid winding for successive iterations of the Poincaré map. Results of a numerical study of the dynamics are discussed and illustrated in detail, including the parameter plane charts of dynamic regimes, bifurcation diagrams, portraits of the attractors of the flow system and of the Poincaré map. On the charts of dynamical regimes, various nontrivial dynamical behaviors take place in a band between the line corresponding to the blue sky catastrophe and the line associated with the Neimark – Sacker bifurcation. Hyperbolic chaos occurs over the entire areas near the blue sky catastrophe line. The destruction of hyperbolic chaos upon departure from these areas in other directions is associated with the emergence of periodic dynamics represented by synchronization tongues in the parameter plane. It is believed possible to implement systems representing the introduced family of dynamical systems as electronic devices. This may be of interest when it comes to constructing electronic generators characterized by insensitivity to variation of parameters, manufacturing errors, interferences etc., since a fundamental attribute of hyperbolic chaos is its property of roughness (structural stability).

APPENDIX

Full systems of ODE which were used in numerical experiments for different values of index m.
$m = 1$

$$
\begin{aligned}
\dot{x}_1 &= \omega_0 y_1 + \Big[1 - (x_2^2 + y_2^2) + \frac{1}{2}(x_1^2 + y_1^2) - \frac{1}{50}(x_1^4 + 2x_1^2 y_1^2 + y_1^4)\Big] x_1 + \frac{1}{2}\varepsilon y_2, \\
\dot{y}_1 &= -\omega_0 x_1 + \Big[1 - (x_2^2 + y_2^2) + \frac{1}{2}(x_1^2 + y_1^2) - \frac{1}{50}(x_1^4 + 2x_1^2 y_1^2 + y_1^4)\Big] y_1, \\
\dot{x}_2 &= \omega_0 y_2 + \Big[(x_1^2 + y_1^2) - \mu + \frac{1}{2}(x_2^2 + y_2^2) - \frac{1}{50}(x_2^4 + 2x_2^2 y_2^2 + y_2^4)\Big] x_2 + \varepsilon x_1, \\
\dot{y}_2 &= -\omega_0 x_2 + \Big[(x_1^2 + y_1^2) - \mu + \frac{1}{2}(x_2^2 + y_2^2) - \frac{1}{50}(x_2^4 + 2x_2^2 y_2^2 + y_2^4)\Big] y_2.
\end{aligned}
\tag{A.1}
$$

$m = 2$

$$\begin{aligned}
\dot{x}_1 &= \omega_0 y_1 + \Big[1 - (x_2^2 + y_2^2) + \frac{1}{2}(x_1^2 + y_1^2) - \frac{1}{50}(x_1^4 + 2x_1^2 y_1^2 + y_1^4)\Big] x_1 + \varepsilon x_2 y_2,\\
\dot{y}_1 &= -\omega_0 x_1 + \Big[1 - (x_2^2 + y_2^2) + \frac{1}{2}(x_1^2 + y_1^2) - \frac{1}{50}(x_1^4 + 2x_1^2 y_1^2 + y_1^4)\Big] y_1,\\
\dot{x}_2 &= \omega_0 y_2 + \Big[(x_1^2 + y_1^2) - \mu + \frac{1}{2}(x_2^2 + y_2^2) - \frac{1}{50}(x_2^4 + 2x_2^2 y_2^2 + y_2^4)\Big] x_2 + \varepsilon x_1,\\
\dot{y}_2 &= -\omega_0 x_2 + \Big[(x_1^2 + y_1^2) - \mu + \frac{1}{2}(x_2^2 + y_2^2) - \frac{1}{50}(x_2^4 + 2x_2^2 y_2^2 + y_2^4)\Big] y_2.
\end{aligned} \tag{A.2}$$

$m = 3$

$$\begin{aligned}
\dot{x}_1 &= \omega_0 y_1 + \Big[1 - (x_2^2 + y_2^2) + \frac{1}{2}(x_1^2 + y_1^2) - \frac{1}{50}(x_1^4 + 2x_1^2 y_1^2 + y_1^4)\Big] x_1 + \frac{1}{2}\varepsilon(3x_2^2 y_2 - y_2^3),\\
\dot{y}_1 &= -\omega_0 x_1 + \Big[1 - (x_2^2 + y_2^2) + \frac{1}{2}(x_1^2 + y_1^2) - \frac{1}{50}(x_1^4 + 2x_1^2 y_1^2 + y_1^4)\Big] y_1,\\
\dot{x}_2 &= \omega_0 y_2 + \Big[(x_1^2 + y_1^2) - \mu + \frac{1}{2}(x_2^2 + y_2^2) - \frac{1}{50}(x_2^4 + 2x_2^2 y_2^2 + y_2^4)\Big] x_2 + \varepsilon x_1,\\
\dot{y}_2 &= -\omega_0 x_2 + \Big[(x_1^2 + y_1^2) - \mu + \frac{1}{2}(x_2^2 + y_2^2) - \frac{1}{50}(x_2^4 + 2x_2^2 y_2^2 + y_2^4)\Big] y_2.
\end{aligned} \tag{A.3}$$

$m = 4$

$$\begin{aligned}
\dot{x}_1 &= \omega_0 y_1 + \Big[1 - (x_2^2 + y_2^2) + \frac{1}{2}(x_1^2 + y_1^2) - \frac{1}{50}(x_1^4 + 2x_1^2 y_1^2 + y_1^4)\Big] x_1 + 2\varepsilon x_2 y_2 (x_2^2 - y_2^2),\\
\dot{y}_1 &= -\omega_0 x_1 + \Big[1 - (x_2^2 + y_2^2) + \frac{1}{2}(x_1^2 + y_1^2) - \frac{1}{50}(x_1^4 + 2x_1^2 y_1^2 + y_1^4)\Big] y_1,\\
\dot{x}_2 &= \omega_0 y_2 + \Big[(x_1^2 + y_1^2) - \mu + \frac{1}{2}(x_2^2 + y_2^2) - \frac{1}{50}(x_2^4 + 2x_2^2 y_2^2 + y_2^4)\Big] x_2 + \varepsilon x_1,\\
\dot{y}_2 &= -\omega_0 x_2 + \Big[(x_1^2 + y_1^2) - \mu + \frac{1}{2}(x_2^2 + y_2^2) - \frac{1}{50}(x_2^4 + 2x_2^2 y_2^2 + y_2^4)\Big] y_2.
\end{aligned} \tag{A.4}$$

ACKNOWLEDGMENTS

The work of SPK and NVS including the model formulation and its qualitative and numerical analysis (Sections 2–5) was supported by RSF grant No 17-12-01008. The work of PVK on Lyapunov analysis and hyperbolicity verification (Section 6) was supported by RFBR grant No 16-02-00135.

REFERENCES

1. Palis, J. and Pugh, C. C., Fifty Problems in Dynamical Systems, in *Dynamical Systems: Proc. Sympos. Appl. Topology and Dynamical Systems (Univ. Warwick, Coventry, 1973/1974): Presented to E. C. Zeeman on His Fiftieth Birthday,* Lecture Notes in Math., vol. 468, Berlin: Springer, 1975, pp. 345–353.
2. Turaev, D. V. and Shil'nikov, L. P., Blue Sky Catastrophes, *Dokl. Math.,* 1995, vol. 51, pp. 404–407; see also: *Dokl. Akad. Nauk,* 1995, vol. 342, no. 5, pp. 596–599.
3. Shil'nikov, L. P. and Turaev, D. V., Simple Bifurcations Leading to Hyperbolic Attractors: Computational Tools of Complex Systems: 1, *Comput. Math. Appl.,* 1997, vol. 34, nos. 2–4, pp. 173–193.
4. Shilnikov, L. P. and Turaev, D. V., A New Simple Bifurcation of a Periodic Orbit of ¡¡Blue Sky Catastrophe¿¿ Type, in *Methods of Qualitative Theory of Differential Equations and Related Topics,* Amer. Math. Soc. Transl. Ser. 2, vol. 200, Providence, R.I.: AMS, 2000, pp. 165–188.
5. Gavrilov, N. and Shilnikov, A., Example of a Blue Sky Catastrophe, in *Methods of Qualitative Theory of Differential Equations and Related Topics,* Amer. Math. Soc. Transl. Ser. 2, vol. 200, Providence, R.I.: AMS, 2000, pp. 99–105.
6. Shilnikov, A. L., Shilnikov, L. P., and Turaev, D. V., Blue-Sky Catastrophe in Singularly Perturbed Systems, *Mosc. Math. J.,* 2005, vol. 5, no. 1, pp. 269–282.
7. Shilnikov, A. and Turaev, D., Blue-Sky Catastrophe, *Scholarpedia,* 2007, vol. 2, no. 8, p. 1889.
8. Shilnikov, L. P., Shilnikov, A. L., and Turaev, D. V., Showcase of Blue Sky Catastrophes, *Internat. J. Bifur. Chaos Appl. Sci. Engrg.,* 2014, vol. 24, no. 8, 1440003, 10 pp.

9. Shilnikov, A. and Cymbalyuk, G., Transition between Tonic Spiking and Bursting in a Neuron Model via the Blue-Sky Catastrophe, *Phys. Rev. Lett.,* 2005, vol. 94, no. 4, 048101, 4 pp.
10. Shilnikov, A., Complete Dynamical Analysis of a Neuron Model, *Nonlinear Dynam.,* 2012, vol. 68, no. 3, pp. 305–328.
11. Barnett, W., O'Brien, G., and Cymbalyuk, G., A Family of Mechanisms Controlling Bursting Activity and Pulse-Triggered Responses of a Neuron Model, in *Proc. of the 29th Southern Biomedical Engineering Conference (SBEC),* 2013, pp. 53–54.
12. Barnett, W. H. and Cymbalyuk, G. S., A Codimension-2 Bifurcation Controlling Endogenous Bursting Activity and Pulse-Triggered Responses of a Neuron Model, *PLoS ONE,* 2014, vol. 9, no. 1, e85451.
13. Glyzin, S. D., Kolesov, A. Yu., and Rozov, N. Kh., The Blue Sky Catastrophe in Relaxation Systems with One Fast and Two Slow Variables, *Differ. Equ.,* 2008, vol. 44, no. 2, pp. 161–175; see also: *Differ. Uravn.,* 2008, vol. 44, no. 2, pp. 158–171, 285.
14. Glyzin, S. D., Kolesov, A. Yu., and Rozov, N. Kh., Blue Sky Catastrophe As Applied to Modeling of Cardiac Rhythms, *Comput. Math. Math. Phys.,* 2015, vol. 55, no. 7, pp. 1120–1137; see also: *Zh. Vychisl. Mat. Mat. Fiz.,* 2015, vol. 55, no. 7, pp. 1136–1155.
15. Bondarev, A. A. and Weigt, H., Sensitivity of Energy System Investments to Policy Regulation Changes: Application of the Blue Sky Catastrophe, https://ssrn.com/abstract=2968230 (May 11, 2017), 23 pp.
16. Maistrenko, Yu. L., Vasylenko, A., Sudakov, O., Levchenko, R., and Maistrenko, V. L., Cascades of Multiheaded Chimera States for Coupled Phase Oscillators, *Internat. J. Bifur. Chaos Appl. Sci. Engrg.,* 2014, vol. 24, no. 8, 1440014, 17 pp.
17. Meca, E., Mercader, I., Batiste, O., and Ramírez-Piscina, L., Blue Sky Catastrophe in Double-Diffusive Convection, *Phys. Rev. Lett.,* 2004, vol. 92, no. 23, 234501, 4 pp.
18. Burgos-García, J. and Delgado, J., On the "Blue Sky Catastrophe" Termination in the Restricted Four-Body Problem, *Celestial Mech. Dynam. Astronom.,* 2013, vol. 117, no. 2, pp. 113–136.
19. Burgos-García, J. and Delgado, J., Periodic Orbits in the Restricted Four-Body Problem with Two Equal Masses, *Astrophys. Space Sci.,* 2013, vol. 345, no. 2, pp. 247–263.
20. Alvarez-Ramírez, M. and Barrabés, E., Transport Orbits in an Equilateral Restricted Four-Body Problem, *Celestial Mech. Dynam. Astronom.,* 2015, vol. 121, no. 2, pp. 191–210.
21. Botha, A. E., Shukrinov, Yu. M., and Kolahchi, M. R., A Farey Staircase from the Two-Extremum Return Map of a Josephson Junction, *Nonlinear Dynam.,* 2016, vol. 84, no. 3, pp. 1363–1372.
22. Hong, L. and Sun, J.-Q., A Fuzzy Blue Sky Catastrophe, *Nonlinear Dynam.,* 2009, vol. 55, no. 3, pp. 261–267.
23. Van Gorder, R. A., Triple Mode Alignment in a Canonical Model of the Blue-Sky Catastrophe, *Nonlinear Dynam.,* 2013, vol. 73, nos. 1–2, pp. 397–403.
24. Leonov, G. A., Cascade of Bifurcations in Lorenz-Like Systems: Birth of a Strange Attractor, Blue Sky Catastrophe Bifurcation, and Nine Homoclinic Bifurcations, *Dokl. Math.,* 2015, vol. 92, no. 2, pp. 563–567; see also: *Dokl. Akad. Nauk,* 2015, vol. 464, no. 4, pp. 391–395.
25. Leonov, G. A., Necessary and Sufficient Conditions of the Existence of Homoclinic Trajectories and Cascade of Bifurcations in Lorenz-Like Systems: Birth of Strange Attractor and 9 Homoclinic Bifurcations, *Nonlinear Dynam.,* 2016, vol. 84, no. 2, pp. 1055–1062.
26. Battelli, F. and Feckan, M., Blue Sky-Like Catastrophe for Reversible Nonlinear Implicit ODEs, *Discrete Contin. Dyn. Syst. Ser. S,* 2016, vol. 9, no. 4, pp. 895–922.
27. Kuznetsov, S. P., Example of a Physical System with a Hyperbolic Attractor of the Smale – Williams Type, *Phys. Rev. Lett.,* 2005, vol. 95, no. 14, 144101, 4 pp.
28. Kuznetsov, S. P. and Seleznev, E. P., Strange Attractor of Smale – Williams Type in the Chaotic Dynamics of a Physical System, *J. Exp. Theor. Phys.,* 2006, vol. 102, no. 2, pp. 355–364; see also: *Zh. Èksper. Teoret. Fiz.,* 2006, vol. 129, no. 2, pp. 400–412.
29. Kuznetsov, S. P. and Pikovsky, A., Autonomous Coupled Oscillators with Hyperbolic Strange Attractors, *Phys. D,* 2007, vol. 232, no. 2, pp. 87–102.
30. Kuznetsov, S. P., *Dynamical Chaos,* 2nd ed., Moscow: Fizmatlit, 2006 (Russian).
31. Kuznetsov, A. P., Kuznetsov, S. P., Sataev, I. R., and Chua, L. O., Two-Parameter Study of Transition to Chaos in Chua's Circuit: Renormalization Group, Universality and Scaling, *Internat. J. Bifur. Chaos Appl. Sci. Engrg.,* 1993, vol. 3, no. 4, pp. 943–962.
32. Isaeva, O. B., Kuznetsov, S. P., and Mosekilde, E., Hyperbolic Chaotic Attractor in Amplitude Dynamics of Coupled Self-Oscillators with Periodic Parameter Modulation, *Phys. Rev. E,* 2011, vol. 84, no. 1, 016228, 10 pp.
33. Kuznetsov, S. P., Example of Blue Sky Catastrophe Accompanied by a Birth of Smale – Williams Attractor, *Regul. Chaotic Dyn.,* 2010, vol. 15, nos. 2–3, pp. 348–353.
34. Kuznetsov, A. P., Kuznetsov, S. P., and Stankevich, N. V., Four-Dimensional System with Torus Attractor Birth via Saddle-Node Bifurcation of Limit Cycles in Context of Family of Blue Sky Catastrophes, *Izv. Vyssh. Uchebn. Zaved. Prikl. Nelin. Dinam.,* 2015, vol. 23, no. 4, pp. 32–39.
35. Isaeva, O. B., Kuznetsov, S. P., and Sataev, I. R., A "saddle–node" Bifurcation Scenario for Birth or Destruction of a Smale – Williams Solenoid, *Chaos,* 2012, vol. 22, no. 4, 043111, 7 pp.

36. Benettin, G., Galgani, L., Giorgilli, A., and Strelcyn, J.-M., Lyapunov Characteristic Exponents for Smooth Dynamical Systems and for Hamiltonian Systems: A Method for Computing All of Them: P. 1: Theory, *Meccanica,* 1980, vol. 15, pp. 9–20.
37. Shimada, I. and Nagashima, T., A Numerical Approach to Ergodic Problem of Dissipative Dynamical Systems, *Progr. Theoret. Phys.,* 1979, vol. 61, no. 6, pp. 1605–1616.
38. Kaplan, J. L. and Yorke, J. A., A Chaotic Behavior of Multi-Dimensional Differential Equations, in *Functional Differential Equations and Approximations of Fixed Points,* H.-O. Peitgen, H.-O. Walther (Eds.), Lecture Notes in Math., vol. 730, Berlin: Springer, 1979, pp. 204–227.
39. Kuptsov, P. V., Fast Numerical Test of Hyperbolic Chaos, *Phys. Rev. E,* 2012, vol. 85, no. 1, 015203, 4 pp.
40. Kuptsov, P. V. and Parlitz, U., Theory and Computation of Covariant Lyapunov Vectors, *J. Nonlinear Sci.,* 2012, vol. 22, no. 5, pp. 727–762.
41. Katok, A. and Hasselblatt, B., *Introduction to the Modern Theory of Dynamical Systems,* Encyclopedia Math. Appl., vol. 54, Cambridge: Cambridge Univ. Press, 1995.
42. *Dynamical Systems 9: Dynamical Systems with Hyperbolic Behaviour,* D. V. Anosov (Ed.), Encyclopaedia Math. Sci., vol. 66, Berlin: Springer, 1995.